IEEE Access
Multidisciplinary | Rapid Review | Open Access Journal

Received January 7, 2022, accepted January 19, 2022, date of publication February 2, 2022, date of current version February 7, 2022.

Digital Object Identifier 10.1109/ACCESS.2022.3146429

Design of a High-Gain Single Circular Patch Radiator With a Cavity-Backed Structure Using Multiple SIW Feeders for Monopulse DF-Applications

SANGWOON YOUN[1], TAE HEUNG LIM[1], BYUNG-JUN JANG[2], (Senior Member, IEEE), AND HOSUNG CHOO[1], (Senior Member, IEEE)

[1]Department of Electronic and Electrical Engineering, Hongik University, Seoul 04066, South Korea
[2]Department of Electrical Engineering, Kookmin University, Seoul 02707, South Korea

Corresponding author: Tae Heung Lim (qpzm0105@mail.hongik.ac.kr)

This work was supported by the Samsung Research Funding Center of Samsung Electronics under Project SRFC-IT1801-51.

ABSTRACT This paper proposes the design of a gain enhanced single circular patch radiator (SCPR) with a cavity-backed structure using multiple substrate integrated waveguide (SIW) feeders for monopulse systems. We derive the equations of a radiation pattern for the multi-feed SCPR and compare it with the full EM simulation results. Based on the theoretical results, the proposed SCPR with multiple feeds is designed by adding the cavity-backed structure to obtain high gain characteristics. In the feeding network, four SIW structures are designed and circularly arranged, which can reduce loss and mutual coupling. Each pair of the SIW feeders can provide sum (Σ) and difference (Δ) patterns to achieve the monopulse direction finding (DF) properties in both elevation and azimuth directions. To verify the feasibility, the proposed antenna is fabricated, and the antenna characteristics are measured. The measured reflection coefficient is -14.5 dB at 5.8 GHz, and the maximum gains are 4.9 dBi and 4.8 dBi in *zy*-plane. To observe the monopulse DF, the estimated direction of arrival (DOA) results are examined in both elevation and azimuth directions. In the whole estimated angle range, the estimation error is lower than 0.49, and the average error is 0.26.

INDEX TERMS Monopulse antenna, single circular patch radiator, multiple SIW feeding network, circular patch cavity model.

I. INTRODUCTION

A monopulse system is one of the accurate and rapid direction finding (DF) systems for target tracking in radar and satellite technologies [1]–[5]. The monopulse system conventionally consists of an array antenna and pattern comparator that can compare the received signal simultaneously from the sum (Σ) and difference (Δ) channels [6], [7]. In general, the monopulse system requires four antenna elements to estimate a direction of arrival (DOA) for both azimuth and elevation directions. For an accurate monopulse DF, the antenna element requires a high bore-sight gain that can increase the ratio between the Σ- and Δ- patterns [8]–[10]. To obtain a high gain property, many studies on various radiator designs of monopulse system have been conducted by employing a horn antenna structure [11], [12], a slotted antenna structure [13]–[16], and a printed Yagi-Uda structure [17], [18]. Although these approaches can result in a high gain performance, the physical size of the antenna radiators are too bulky to implement in small platforms in various industrial fields, such as smart devices, small drones, and IoT applications. To overcome the problem, comprehensive efforts have been devoted to miniaturizing the radiator geometry, i.e., using a corrugated structure for a horn antenna [19], a high dielectric material for a patch [20], [21], and a slot loaded patch antenna [22], [23]. However, multiple radiators with complicated feeding structures and expensive fabrication costs are still required for the monopulse array antenna to estimate both azimuth and elevation angles.

The associate editor coordinating the review of this manuscript and approving it for publication was Kwok Chung.

In this paper, we propose a high-gain single circular patch radiator (SCPR) with a cavity-backed structure using multiple substrate integrated waveguide (SIW) feeders for monopulse direction finding (DF) applications. To obtain theoretical insights, we derive equations of a radiation pattern for the multi-feed SCPR based on the cavity model theory of the circular patch antenna with a single feed. The calculated radiation patterns for the SCPR with the multiple feeders are compared with the full EM simulation results for the circular patch antenna under the assumption of an infinite ground and substrate. Based on the cavity model results, the proposed SCPR is designed with the multiple SIW feeding network to minimize the distortion of the radiation patterns [24], [25]. In addition, a cavity-backed structure is added to the SCPR to obtain the high bore-sight gain by reducing the back-radiation in the radiation pattern. In the feeding network, four SIW structures are designed to excite the fundamental mode to the SCPR and are circularly arrayed with an interval of 90°. This feeding network can reduce transmission losses and mutual couplings between the adjacent ports. Each pair of the SIW feeders can provide Σ- and Δ-patterns in the azimuth and elevation directions to achieve the monopulse DF properties. To verify the feasibility, the proposed antenna is fabricated, and the antenna characteristics such as reflection coefficients, bore-sight gains, mutual couplings, and radiation patterns are measured in a full anechoic chamber. To observe the monopulse DF performance, the DOA estimation results using the monopulse amplitude comparison method are obtained by adopting the ratio of the Σ- and Δ-patterns in both azimuth and elevation directions. The results demonstrate that the proposed SCPR with multiple SIW feed structures is suitable for small monopulse DF applications.

II. PROPOSED ANTENNA WITH THE SIW FEEDING NETWORK

A. THEORETICAL APPROACH USING MULTI-FEED CAVITY MODEL

Fig. 1(a) shows the conceptual geometry of a microstrip circular patch antenna with a cavity model for a single feed excitation. The circular patch with a radius of a is printed on an infinite substrate with a height of h. The substrate has a dielectric constant of ε_r, and the ground of the antenna is also assumed to be infinite. These conditions allow the circumferential wall of the circular patch to be treated as a perfect magnetic conduction boundary by using the cavity model with the surface equivalent magnetic current density M_ϕ When assuming the TM_{11} mode field distribution under the patch radiator, the electric fields in the radial direction can be expressed using equations (1) to (4), as follows [24]:

$$E_z = E_0 J_1\left(k_0\rho'\right)\cos\phi', \tag{1}$$

$$M_\phi = a_\phi 2E_0 J_1\left(ka_e\right)\cos\phi', \tag{2}$$

$$a_e = a\left\{1+\frac{2h}{\pi a\varepsilon_r}[\ln(\frac{\pi a}{2h})+1.7726]\right\}^{1/2}, \tag{3}$$

$$V_0 = hE_0 J_1\left(k_0 a_e\right), \tag{4}$$

where E_z is an electric field intensity along z-axis direction, and a_e is an effective radius considering the substrate, and k_0 is a propagation constant. V_0 is the voltage induced from the uniform magnetic current as an approximation of a circular loop at $\phi' = 0°$. In our research, the single feed circular patch with the cavity model is extended to the multi-feed with a single patch radiator. Fig. 1(b) presents the conceptual geometry of the SCPR with the multiple feeding ports. All ports (total number of N) are circularly arranged and located at a uniform distance of d from the center of the patch antenna. Each port (port number n) has an angular position of ϕ'_n on the xy-plane. The surface equivalent magnetic current density M^n_ϕ induced from each port can be calculated using the cavity model. From the magnetic current density, the radiating electric field is then obtained using the radiation equation for the circular aperture (5) to (9) [24].

$$L^n_\theta = \int_S\int M^n_\phi \cos\theta \sin\left(\phi-\phi'_n\right) e^{jkr'\cos\psi} ds', \tag{5}$$

$$L^n_\phi = \int_S\int M^n_\phi \cos\left(\phi-\phi'_n\right) e^{jkr'\cos\psi} ds', \tag{6}$$

$$E^n_\theta \simeq -\frac{jke^{-jkr}}{4\pi r}\left(L^n_\phi\right), \tag{7}$$

$$E^n_\phi \simeq +\frac{jke^{-jkr}}{4\pi r}\left(L^n_\theta\right), \tag{8}$$

$$\beta_d = -\frac{k_0}{2}\frac{d}{\sqrt{\varepsilon_{reff}}}, \tag{9}$$

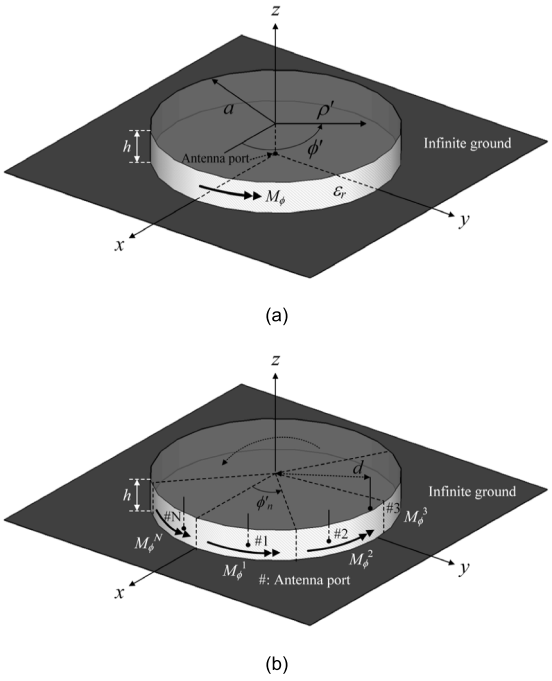

FIGURE 1. Cavity model and equivalent magnetic current density for the SCPR. (a) Single feed model. (b) Multi-feed model.

where β_d is the phase difference of the magnetic current density between the adjacent ports, and ε_{reff} is the effective dielectric constant in terms of ε_r expressed as [26], [27]:

$$\varepsilon_{reff} = \frac{\varepsilon_r + 1}{2} + \frac{\varepsilon_r - 1}{2}\left[1 + 12\frac{h}{a_e}\right]^{-1/2}. \quad (10)$$

Therefore, the final forms of the electric field according to the θ and ϕ directions can be denoted in the equations (11) to (14) [28].

$$E_\theta^n = -j\frac{k_0 a_e V_0 e^{-jk_0 r}}{2r}\{\cos\phi D^n\}, \quad (11)$$

$$E_\phi^n = j\frac{k_0 a_e V_0 e^{-jk_0 r}}{2r}\{\cos\theta \sin\phi S^n\}, \quad (12)$$

$$D^n = J_0(k_0 a_e \beta_d \cos\phi_n' \sin\theta) - J_2(k_0 a_e \beta_d \cos\phi_n' \sin\theta), \quad (13)$$

$$S^n = J_0(k_0 a_e \beta_d \cos\phi_n' \sin\theta) + J_2(k_0 a_e \beta_d \cos\phi_n' \sin\theta), \quad (14)$$

where E_θ^n and E_ϕ^n are the θ and ϕ-components of the electric field in the far-zone, and r is the distance to the observation point. J_m is the Bessel function of the first kind in the m^{th} order, and D^n and S^n represent the difference and sum of the Bessel functions of J_0 and J_2. In Bessel function, the phase difference (β_d) and the angular position ($\cos\phi_n'$) terms are included to derive the radiation electric field pattern considering the location of the multiple port excitations. To verify the theoretical derivations, we compare the EM simulation and the theoretical calculation of the normalized electric field as shown in Fig. 2. The comparative model is designed with variables $a = 10.5$ mm, $h = 1.6$ mm, $d = 1.5$ mm, and $\varepsilon_r = 2.2$. The solid and dotted lines denote normalized electric fields in zx- and zy-planes based on the proposed theory. Dashed lines and dash-dotted lines show the results using the full-wave EM simulation. In EM simulation, the circular patch antenna is designed as a perfect electric conductor on an infinite substrate with a ground plate to similarly design the theoretical model. The electric field result is symmetric in zy-plane; on the other hand, the results in zx-plane are slightly steered to the positive azimuth direction due to the effect of the multi ports.

B. IMPLEMENTATION USING THE SIW MULTI-FEED NETWORK

Fig. 3 illustrates the geometry of the proposed circular patch antenna with the multi-port SIW feeding network based on the theoretical results. The proposed antenna is composed of the single patch radiator, the cavity-backed structure, and the four SIW feeders. To design the single radiator, the circular patch having a diameter of d_1 is printed on a TLY-5 substrate ($\varepsilon_r = 2.2$, $\tan\delta = 0.0009$) that has a diameter of d_2 and a height of h_1. The circumference of the cylinder substrate is surrounded by the cavity-backed structure with a height of h_2 and the ground plate. To assemble and fix the multi-feed network, a cross-groove on the cavity-backed

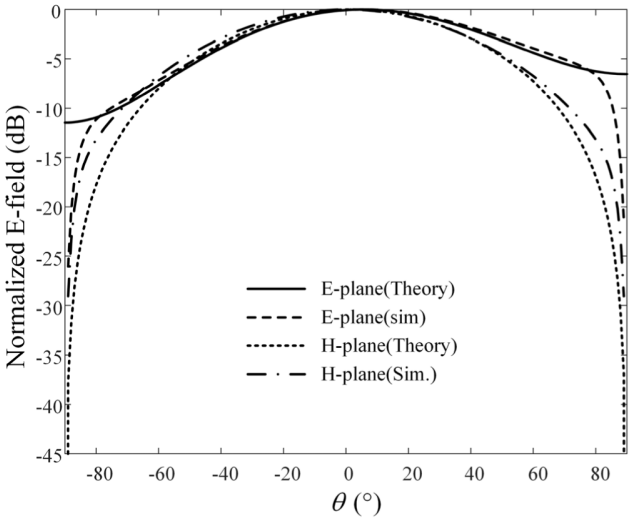

FIGURE 2. Comparison of far-zone electric fields between the theoretical calculations and the full-wave EM simulation results.

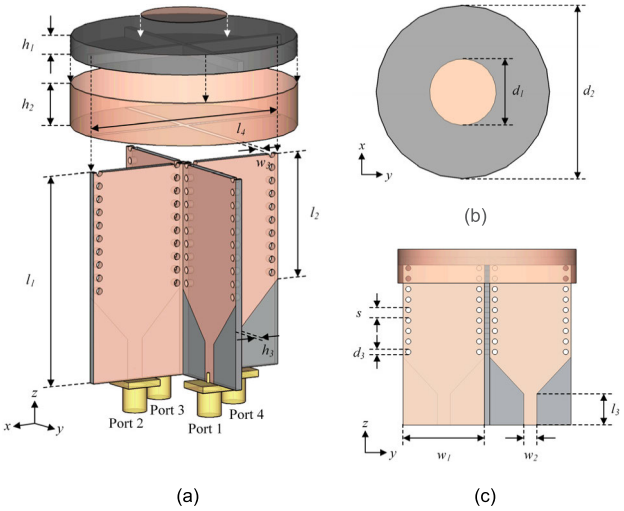

FIGURE 3. The geometry of the proposed antenna. (a) Isometric view. (b) Top view. (c) Side view.

TABLE 1. Design parameters of the proposed antenna.

Parameters	Optimized values
h_1	3.2 mm
h_2	6.5 mm
h_3	1.6 mm
l_1	43 mm
l_2	28 mm
d_1	22 mm
d_2	50 mm
s	2 mm
d_3	1 mm
w_1	21.2 mm
w_2	3 mm
l_3	4 mm

structure is designed with a width of w_3 and a length of l_4. The distance from the ground to the radiator is designed

to be about $\lambda/4$ to increase the radiation directivity, and the low mutual coupling characteristics of the proposed antenna can be obtained by shorting the cavity with the ground. To design the multi-feed network, four identical TE_{10} mode SIWs are employed according to the following equation with the width w of the fundamental rectangular waveguide (15) [29].

$$w_1 = w - 1.08\frac{d_3^2}{s} + 0.1\frac{d_3^2}{w}, \tag{15}$$

where s is the interval of the adjacent SIW via holes, and d_3 is the diameter of the SIW via holes. The SIW feeder has the dimensions of width $\times$ height $\times$ thickness ($w_1 \times l_1 \times h_3$). SIW structures preserve most of the advantages of conventional metallic waveguides, while realizing low loss performance in a compact size with low-cost. In addition, the SIW, which has a full-closed structure, is able to avoid the additional radiation coupling and interferences [30], [31]. To have a transition between the connector and the waveguide, the linear transition microstrip line is employed on the top plane of the SIW, where the feeding line excited by an SMA connector has a width of w_2 and a length of l_3. Each SIW port is circularly arrayed for the four-port network, which can have low transmission losses and mutual coupling characteristics. The detailed design parameters are listed in Table 1.

C. FABRICATION AND MEASUREMENT

Fig. 4(a) shows the photographs of the fabricated antenna for each component: the circular patch antenna, the cavity-backed structure, and the SIW feeders. Figs. 4(b) and (c) illustrate the fabrication of the assembled antenna where the SCPR is fed by four-port SIW feeding network in the absence and presence of the cavity-backed structure. Fig. 5 presents the measured and simulated reflection coefficients of the proposed antenna for the port 1 with and without the cavity-backed structure. For the cavity-backed antenna, the measurement (solid line) and the simulation (dashed line) results are -14.5 dB and -10.1 dB at 5.8 GHz, respectively. The measured (dotted line) and simulated (dash-dotted line) reflection coefficients for the absence of the cavity agree well with each other, and those values are -5.0 dB and -3.7 dB at 5.8 GHz, respectively. Note that the resonant frequency is dominantly determined by the SIW dimensions, and the level of the bore-sight gain is mostly affected by changing the patch radiator diameter. Fig. 6 presents the measured mutual coupling between the adjacent ports (port 1 and port 2) in comparison with the simulation in terms of the cavity existence. The proposed antenna with the cavity-backed structure has the measured and simulated mutual couplings of -11.8 dB and -13.8 dB at 5.8 GHz. On the other hand, the SCPR without the cavity has the higher measured and simulated mutual couplings of -10.6 dB and -6.2 dB compared to the proposed structure. In the measurement and simulation setups, port 1 of the proposed antenna is excited, and the other ports are terminated by 50-Ω loads to obtain the gains of the active element pattern. Fig. 7 depicts the simulated and measured bore-sight gains of port 1 for the proposed antenna with and without a cavity-backed structure. The measured and simulated results of the proposed antenna are 3.1 dBi and 3.8 dBi at 5.8 GHz, and those of the absence for the cavity are -8.1 dBi and -4.4 dBi at 5.8 GHz, respectively. Figs. 8(a) to (d) show the measured and simulated 2D active element patterns for each port of the proposed antenna. Port 1 and port 3 have the measured maximum gains of 4.9 dBi and 4.8 dBi at $\theta = -22°$ and 22° in zy-plane, while port 2 and port 4 have those of 4.7 dBi and 4.8 dBi at $\theta = -23°$ and 25° in zx-plane. For all ports, the measured cross polarization levels are higher than 16 dB at the maximum gain directions. Figs. 8(e) to (h) present the 2D active element patterns of another model for each port. All ports have the maximum gains of 6 dB lower than those of the proposed antenna. We also measure 3D radiation patterns to observe the antenna pattern shape for each port, as shown in Fig. 9. The tilt of the active element pattern is occurred by the locations of the feeding points, the asymmetric structure of the feeding network in the measurement setup, and the mutual couplings. The array distance between the adjacent ports is a dominant parameter that affects the tilt angle of the active element pattern. For example, if the array distance is large enough, the active element pattern will become similar to a stand-alone antenna pattern. Thus, these tilted active element patterns directly affect the monopulse Σ- and Δ-patterns. When the tilt angles of the active element patterns are small, then the Σ-pattern can have a narrow beam width. In the same manner, the Δ-pattern can have a deep null depth. In addition, we simulated the proposed antenna to explain the field transition mechanism. Fig. 10(a) shows the simulated E-field distributions of the proposed antenna. The TE_{10} mode E-field excited by the SIW feeder is gradually converted to the TM_{11} mode of the circular patch radiator in the cavity-backed structure. Then, as shown in Fig. 10(b) and (c), the simulated H-field and surface current distribution confirm that the proposed antenna is operated as the TM_{11} mode, which is obviously similar to the theoretical results of the TM_{110} mode for the cavity model [32], [33]. The results demonstrate that the SIW multi-feeding network is appropriate with the proposed SCPR.

III. MONOPULSE DOA ESTIMATION

In general, the monopulse amplitude comparison method is used to estimate a signal direction using four squinted beams that are simultaneously generated. This method computes the amplitudes of Σ- and Δ-patterns. Then, the ratio between the Σ- and Δ-patterns, so called monopulse ratio, is calculated to estimate the angle direction of the received signal. For example, when a target is located on the bore-sight direction of the antenna, the monopulse ratio becomes zero. However, when the target is off the bore-sight direction, the monopulse ratio increases [34]. In the proposed

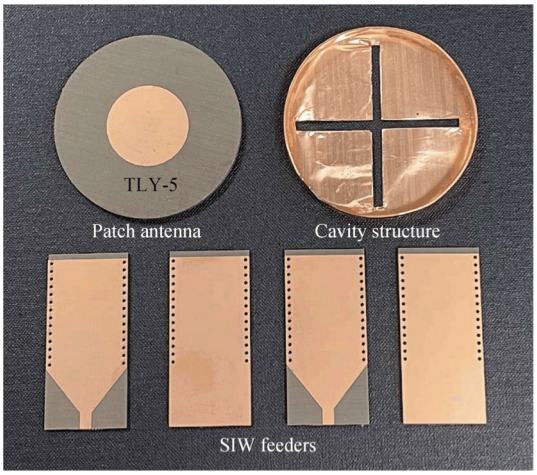

(a)

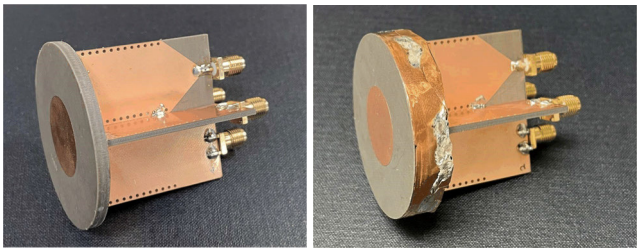

(b) (c)

FIGURE 4. Photographs of the fabricated antenna. (a) Antenna components. (b) Assembled antenna without a cavity-backed structure. (c) Assembled antenna with a cavity-backed structure.

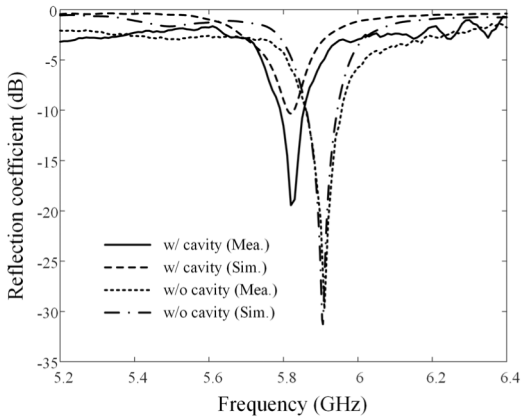

FIGURE 5. Simulated and measured reflection coefficients for w/ and w/o a cavity-backed structure.

multi-feeding network, port 1 and port 3 are used to have sum and difference patterns for the azimuth angle direction. Port 2 and port 4 are utilized to obtain the same pattern characteristics for elevation angle direction estimation. Fig. 11 presents the Σ- and Δ-patterns in *zx*- and *zy*-planes for the monopulse direction finding using the proposed antenna. The solid, dashed, dotted, and dash-dotted lines indicate the Σ- and Δ-patterns in *zx*- and *zy*-planes, respectively. To clearly observe the DOA estimation, the measured data of the radiation patterns are compensated by employing a

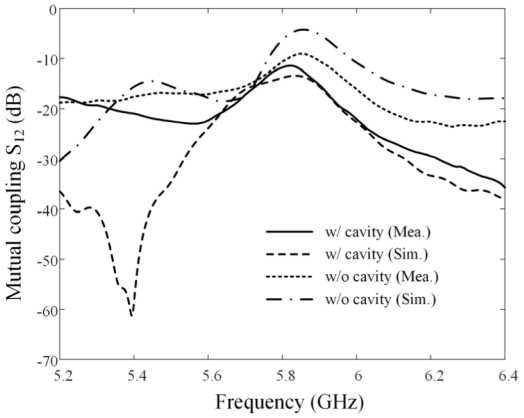

FIGURE 6. Simulated and measured mutual couplings for w/ and w/o a cavity-backed structure.

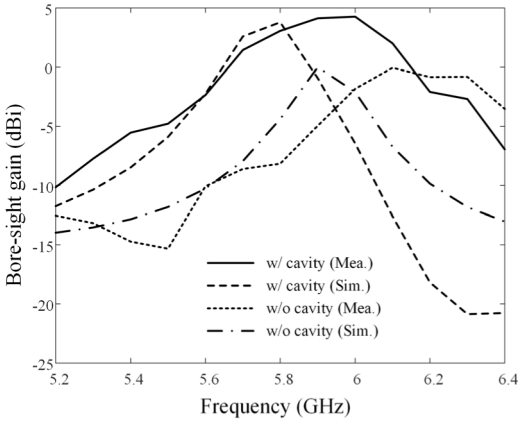

FIGURE 7. Simulated and measured bore-sight gains for w/ and w/o a cavity-backed structure.

TABLE 2. Antenna performances of the proposed antenna with some previous studies.

	Proposed antenna	[4]	[13]	[18]
Antenna type	**Patch**	Horn	Slot	Yagi
Operating frequency	**5.8 GHz**	7.7-8.5 GHz	60 GHz	9.4-10.05 GHz
The number of radiators	**1**	5	16	4
Aperture size	**0.96 λ**	4.9 λ	4 λ	4 λ
Antenna length	**0.9 λ**	9.7 λ	10.6 λ	4 λ
Null depth	**-34.1 dB**	-20 dB	-31 dB	-33.8 dB
Detectable direction	**Az & El**	Az & El	Az & El	Az

moving average filter to smooth the fluctuating noises [35], where the window size is 5. The null depths of the Δ-patterns

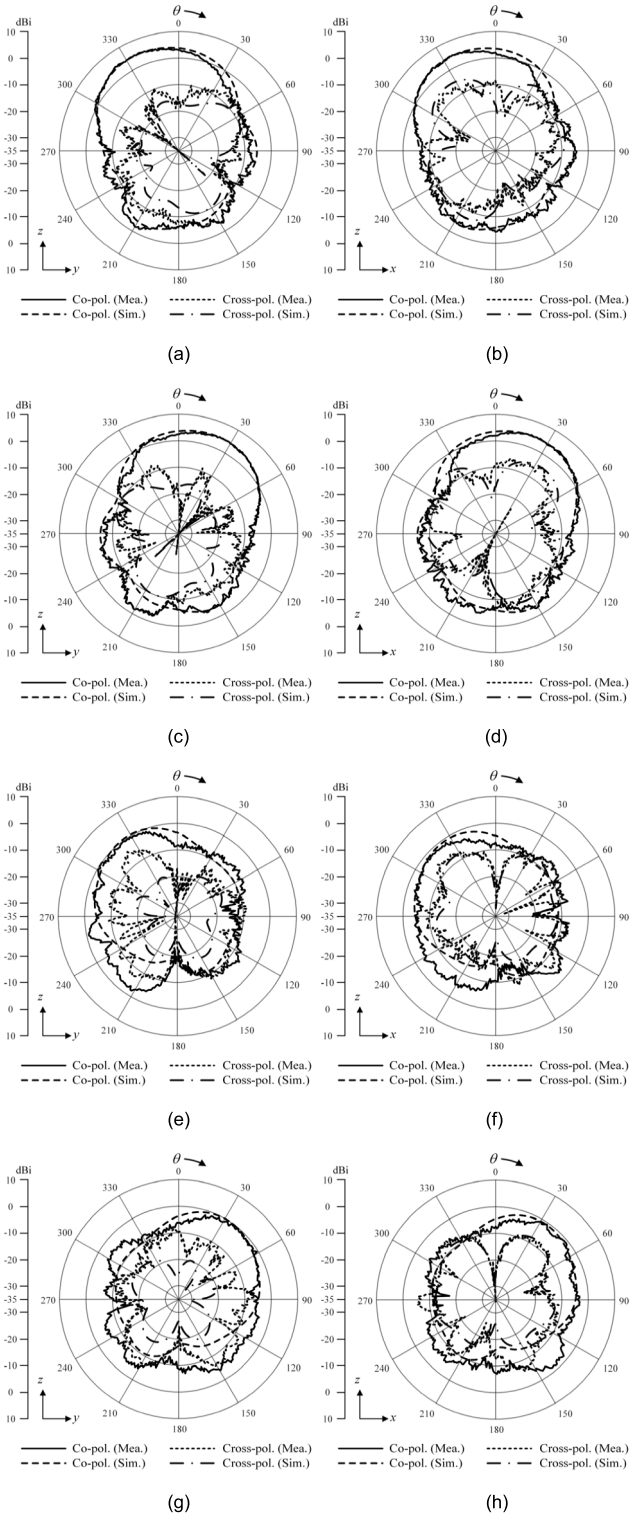

FIGURE 8. Simulated and measured radiation patterns of the proposed antenna. (a) Port 1. (b) Port 2. (c) Port 3. (d) Port 4 (w/ the cavity-backed structure). (e) Port 1. (f) Port 2. (g) Port 3. (h) Port 4 (w/o the cavity-backed structure).

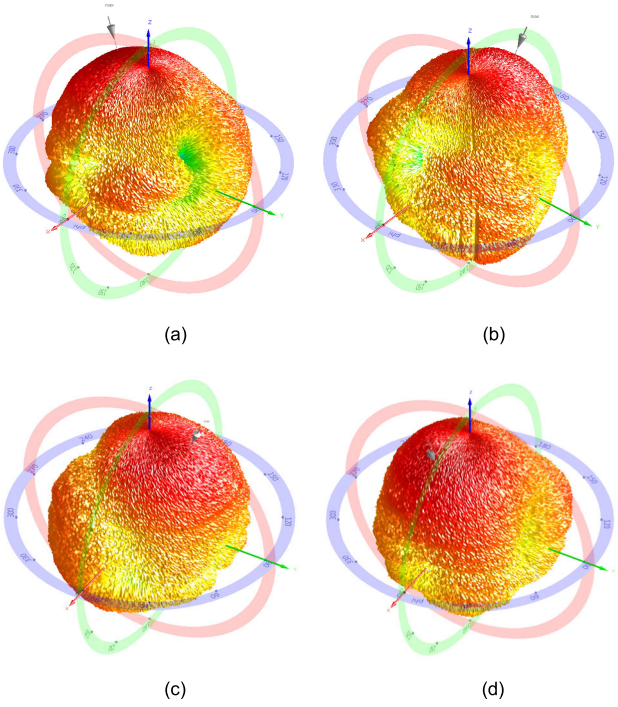

FIGURE 9. Measured 3D radiation patterns of the proposed antenna. (a) Port 1. (b) Port 2. (c) Port 3. (d) Port 4 (w/ the cavity-backed structure).

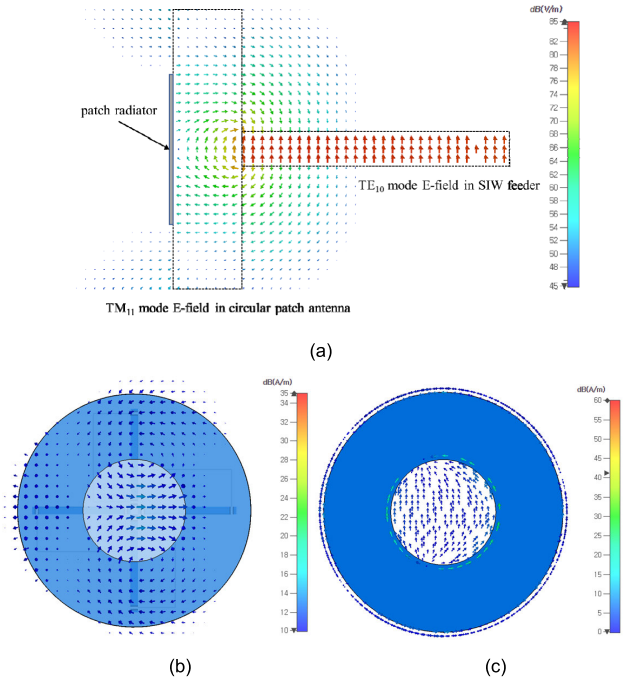

FIGURE 10. Field and current distribution of the proposed antenna. (a) E-field for the transition from SIW feeder to SCPR. (b) Magnetic field. (c) Surface current density.

in the *zx*- and *zy*-planes are −34.1 dB and −32.8 dB at the angle of 1° and 3°, respectively. Herein, the maximum deviations between the Σ- and Δ-patterns are 44 dB and 44.5 dB in *zx*- and *zy*-planes within the angle range from -30° to 30°. To further analyze the DOA estimation, the monopulse

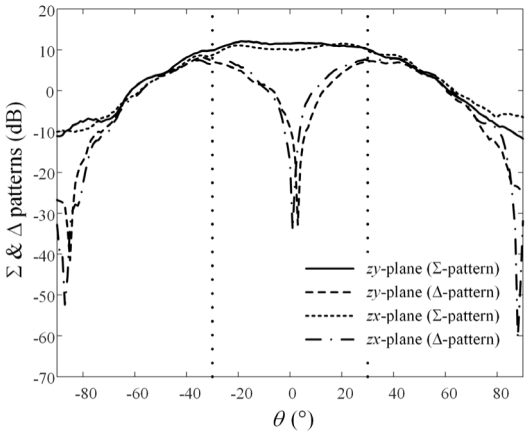

FIGURE 11. Calculated sum (Σ) and difference (Δ) patterns of the proposed monopulse antenna.

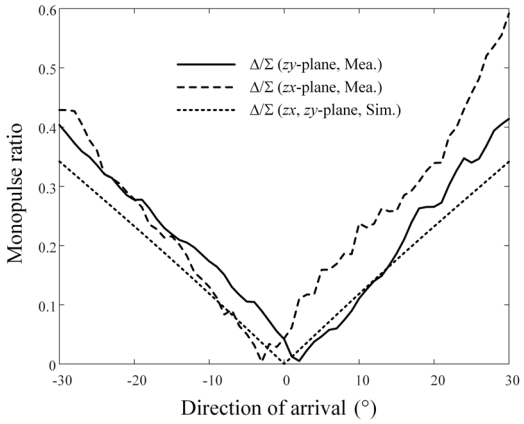

FIGURE 12. Simulated and measured monopulse ratio of the proposed antenna.

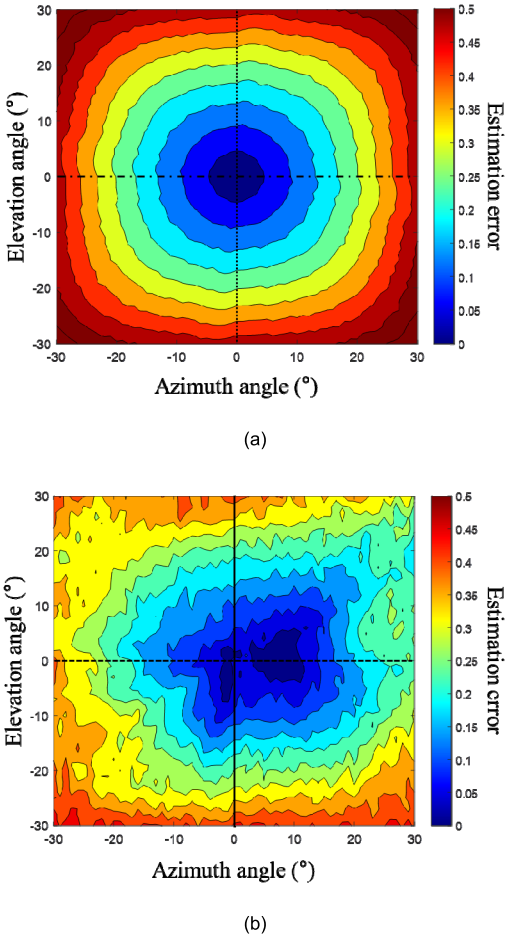

FIGURE 13. 2D monopulse ratio estimation error map according to the DOA in the azimuth and elevation direction. (a) Usage of the simulated patterns. (b) Usage of the measured patterns.

ratios in the azimuth and elevation directions are calculated using the simulated and measured active element patterns, as shown in Fig. 12. The solid, dashed, and dotted lines represent the measured monopulse ratio results in *zy*- and *zx*-planes and the simulation results. Zero value of the measured monopulse ratio is slightly shifted from the bore-sight DOA because of the tilted null direction of the difference pattern, and the fluctuations of the measured DOA estimation results are caused by the shape of the measured patterns. In addition, the estimation errors between the monopulse ratios using the ideal isotropic pattern and the proposed antenna patterns are obtained in the azimuth and elevation angles. Fig. 13 illustrates the 2D estimation error map calculated based on the simulated and measured radiation patterns. The simulated and measured 2D estimation error map results show a similar tendency that the errors gradually become large when increasing the DOA angles. A large estimation error value is observed at DOA of 30° because the sum and difference patterns of the patch antenna are more sharply curved than those of the ideal isotropic sources. In addition, the minimum and average estimation errors are 0.49 and 0.26 in the whole estimated angle ranges. The proposed antenna has a null depth of −34.1 dB using only a single radiator, and it can achieve the monopulse direction finding estimations in both azimuth and elevation directions with the SIW feeding network, as listed in Table 2.

IV. CONCLUSION

In this paper, the high-gain SCPR with a cavity-backed structure using multiple SIW feeders was proposed for monopulse DF applications. To obtain theoretical insights, the radiation pattern equations for the multi-feed SCPR were derived based on the cavity model theory of the circular patch antenna with a single feed. Based on the theoretical results, the proposed SCPR was designed with four SIW feeding networks with a cavity-backed structure to obtain the high gain property. To verify the feasibility, the proposed antenna was fabricated and measured in a full anechoic chamber to obtain the antenna characteristics. The measured reflection coefficient and the mutual coupling of the proposed antenna were −14.5 dB

and −11.8 dB at 5.8 GHz. The maximum gains for port 1 and port 3 were 4.9 dBi and 4.8 dBi at −22° and 22° in zy-plane, respectively. To observe the monopulse DF for the proposed antenna, the DOA estimation results using the monopulse amplitude comparison were obtained by adopting the ratio of the Σ and Δ patterns in both the azimuth and elevation directions. In the whole estimated angle range, the estimation error was lower than 0.49, and the average error was 0.26.

REFERENCES

[1] C. Kumar, V. S. Kumar, and V. V. Srinivasan, "Design aspects of a compact dual band feed using dielectric rod antennas with multiple element monopulse tracking," *IEEE Trans. Antennas Propag.*, vol. 61, no. 10, pp. 4926–4932, Oct. 2013.

[2] R. Feng, F. Uysal, P. Aubry, and A. Yarovoy, "MIMO–monopulse target localization for automotive radar," *IET Radar Sonar Navigat.*, vol. 12, no. 10, pp. 1131–1136, Oct. 2018.

[3] S.-I. Jeon, Y.-W. Kim, and D.-G. Oh, "A new active phased array antenna for mobile direct broadcasting satellite reception," *IEEE Trans. Broadcast.*, vol. 46, no. 1, pp. 34–40, Mar. 2000.

[4] S. S. Roy, C. Saha, T. Nagasekhar, S. B. Mane, C. S. Padmavathy, G. Umadevi, and M. N. Kumar, "Design of a compact multielement monopulse feed for ground-station satellite tracking applications," *IEEE Antennas Wireless Propag. Lett.*, vol. 18, no. 9, pp. 1721–1725, Sep. 2019.

[5] J.-H. Nam, J.-W. Rim, H. Lee, I.-S. Koh, and J.-H. Song, "Modeling of monopulse radar signals reflected from ground clutter in a time domain considering Doppler effects," *J. Electromagn. Eng. Sci.*, vol. 20, no. 3, pp. 190–198, Jul. 2020.

[6] E. Mosca, "Angle estimation in amplitude comparison monopulse systems," *IEEE Trans. Aerosp. Electron. Syst.*, vol. AES-5, no. 2, pp. 205–212, Mar. 1969.

[7] E. Hofstetter and D. Delong, "Detection and parameter estimation in an amplitude-comparison monopulse radar," *IEEE Trans. Inf. Theory*, vol. IT-15, no. 1, pp. 22–30, Jan. 1969.

[8] N. Wong, R. Tang, and E. Barber, "A multielement high power monopulse feed with low sidelobe and high aperture efficiency," *IEEE Trans. Antennas Propag.*, vol. AP-22, no. 3, pp. 402–407, May 1974.

[9] J. Zhao, H. Li, X. Yang, W. Mao, B. Hu, T. Li, H. Wang, Y. Zhou, and Q. Liu, "A compact Ka-band monopulse Cassegrain antenna based on reflectarray elements," *IEEE Antennas Wireless Propag. Lett.*, vol. 17, no. 2, pp. 193–196, Feb. 2018.

[10] A. Vosoogh, A. Haddadi, A. U. Zaman, J. Yang, H. Zirath, and A. A. Kishk, "W-band low-profile monopulse slot array antenna based on gap waveguide corporate-feed network," *IEEE Trans. Antennas Propag.*, vol. 66, no. 12, pp. 6997–7009, Dec. 2018.

[11] H. Z. Zhang, C. Granet, and M. A. Sprey, "A compact Ku-band monopulse horn," *Microw. Opt. Technol. Lett.*, vol. 34, no. 1, pp. 9–13, Jul. 2002.

[12] C. C. Ling and G. M. Rebeiz, "94 GHz integrated horn monopulse antennas," *IEEE Trans. Antennas Propag.*, vol. 40, no. 8, pp. 981–984, Aug. 1992.

[13] J. Zhu, S. Liao, S. Li, and Q. Xue, "60 GHz substrate-integrated waveguide-based monopulse slot antenna arrays," *IEEE Trans. Antennas Propag.*, vol. 66, no. 9, pp. 4860–4865, Sep. 2018.

[14] J. Aliasgari and Z. Atlasbaf, "A novel compact monopulse parallel-plate slot array antenna," *IEEE Antennas Wireless Propag. Lett.*, vol. 15, pp. 762–765, 2016.

[15] A. Ali, H. Wang, Y. Yun, J. Lee, and I. Park, "Compact slot antenna integrated with a photovoltaic cell," *J. Electromagn. Eng. Sci.*, vol. 20, no. 4, pp. 248–253, Oct. 2020.

[16] B. Liu, W. Hong, Z. Kuai, X. Yin, G. Luo, J. Chen, H. Tang, and K. Wu, "Substrate integrated waveguide (SIW) monopulse slot antenna array," *IEEE Trans. Antennas Propag.*, vol. 57, no. 1, pp. 275–279, Jan. 2009.

[17] J. Huang and A. C. Densmore, "Microstrip Yagi array antenna for mobile satellite vehicle application," *IEEE Trans. Antennas Propag.*, vol. 39, no. 7, pp. 1024–1030, Jul. 1991.

[18] X. Zou, C.-M. Tong, J.-S. Bao, and W.-J. Pang, "SIW-fed Yagi antenna and its application on monopulse antenna," *IEEE Antennas Wireless Propag. Lett.*, vol. 13, pp. 1035–1038, 2014.

[19] B. Du, E. K.-N. Yung, K.-Z. Yang, and W.-J. Zhang, "Wideband linearly or circularly polarized monopulse tracking corrugated horn," *IEEE Trans. Antennas Propag.*, vol. 50, no. 2, pp. 192–197, Feb. 2002.

[20] M. Asaadi and A. Sebak, "Gain and bandwidth enhancement of 2 × 2 square dense dielectric patch antenna array using a holey superstrate," *IEEE IEEE Antennas Wireless Propag. Lett.*, vol. 16, pp. 1808–1811, 2017.

[21] S.-C. Tang, X.-Y. Wang, W.-W. Yang, and J.-X. Chen, "Wideband low-profile dielectric patch antenna and array with anisotropic property," *IEEE Trans. Antennas Propag.*, vol. 68, no. 5, pp. 4091–4096, May 2020.

[22] S. Radavaram and M. Pour, "Wideband radiation reconfigurable microstrip patch antenna loaded with two inverted U-slots," *IEEE Trans. Antennas Propag.*, vol. 67, no. 3, pp. 1501–1508, Mar. 2019.

[23] F. Yu, Y. Xie, and L. Zhang, "Single patch antenna with monopulse patterns," *IEEE Microw. Wireless Compon. Lett.*, vol. 26, no. 10, pp. 762–764, Oct. 2016.

[24] D. Deslandes and K. Wu, "Integrated microstrip and rectangular waveguide in planar form," *IEEE Microw. Wireless Compon. Lett.*, vol. 11, no. 2, pp. 68–70, Feb. 2001.

[25] M. Bozzi, A. Georgiadis, and K. Wu, "Review of substrate-integrated waveguide circuits and antennas," *IET Microw., Antennas Propag.*, vol. 5, no. 8, pp. 909–920, Jun. 2011.

[26] C. Balanis, *Antenna Theory*. Hoboken, NJ, USA: Wiley, 1997.

[27] R. Garg, P. Bhartia, I. J. Bahl, and A. Ittipiboon, *Microstrip Antenna Design Handbook*. Norwood, MA, USA: Artech House, 2001.

[28] C. Balanis, *Advanced Engineering Electromagnetics*, 2nd ed. Hoboken, NJ, USA: Wiley, 2012.

[29] F. Xu and K. Wu, "Guided-wave and leakage characteristics of substrate integrated waveguide," *IEEE Trans. Microw. Theory Techn.*, vol. 53, no. 1, pp. 66–73, Jan. 2005.

[30] A. A. Diman, F. Karami, P. Rezaei, A. Amn-e-Elahi, Z. Mousavirazi, T. A. Denidni, and A. A. Kishk, "Efficient SIW-feed network suppressing mutual coupling of slot antenna array," *IEEE Trans. Antennas Propag.*, vol. 69, no. 9, pp. 6058–6063, Sep. 2021.

[31] Y. J. Cheng, W. Hong, and K. Wu, "94 GHz substrate integrated monopulse antenna array," *IEEE Trans. Antennas Propag.*, vol. 60, no. 1, pp. 121–129, Jan. 2012.

[32] F. Ren, W. Hong, and K. Wu, "Three-dimensional SIW-driven microstrip antenna for wideband linear and circular polarization applications," *IEEE Antennas Wireless Propag. Lett.*, vol. 16, pp. 2400–2403, 2017.

[33] H. Iizuka, T. Watanabe, and K. Nishikawa, "Millimeter-wave microstrip line to waveguide transition fabricated on a single layer dielectric substrate," *IEICE Trans. Commun.*, vol. 85, no. 6, pp. 1169–1177, Jun. 2002.

[34] B. R. Mahafza, *Radar Systems Analysis and Design Using MATLAB*, 3rd ed. Boca Raton, FL, USA: CRC Press, 2013.

[35] S. Golestan, M. Ramezani, J. M. Guerrero, F. D. Freijedo, and M. Monfared, "Moving average filter based phase-locked loops: Performance analysis and design guidelines," *IEEE Trans. Power Electron.*, vol. 29, no. 6, pp. 2750–2763, Jun. 2014.

SANGWOON YOUN received the B.S. and M.S. degrees in electronic and electrical engineering from Hongik University, Seoul, South Korea, in 2019 and 2021, respectively, where he is currently pursuing the Ph.D. degree in electronic and electrical engineering. His research interests include EMI and EMC, wave propagation, GPS antennas, 5G application, direction finding, and anti-jamming systems.

TAE HEUNG LIM received the B.S. and M.S. degrees in electronic and electrical engineering from Hongik University, Seoul, South Korea, in 2016 and 2018, respectively, where he is currently pursuing the Ph.D. degree in electronic and electrical engineering. His research interests include global positioning system antennas, time-modulated array, antenna arrays, position optimization of array elements for adaptive beamforming, and wave propagations for radar applications.

BYUNG-JUN JANG (Senior Member, IEEE) received the B.S., M.S., and Ph.D. degrees in electronic engineering from Yonsei University, Seoul, South Korea, in 1990, 1992, and 1997, respectively. From 1995 to 1999, he was with LG Electronics, Seoul, where he developed code-division multiple-access (CDMA) and digital enhanced cordless telecommunication (DECT) RF modules. From 1999 to 2005, he was with the Electronics and Telecommunications Research Institute (ETRI), Daejeon, South Korea, where he performed research in the fields of satellite RF components and monolithic microwave integrated circuits. In 2005, he joined Kookmin University, Seoul, where he is currently with the Department of Electrical Engineering. His research interests include the areas of RF circuit design, radio frequency identification (RFID) system design, wireless power transfer (WPT) system design, frequency interference modeling and spectrum engineering, and wireless sensor design.

HOSUNG CHOO (Senior Member, IEEE) received the B.S. degree in radio science and engineering from Hanyang University, Seoul, South Korea, in 1998, and the M.S. and Ph.D. degrees in electrical and computer engineering from the University of Texas at Austin, in 2000 and 2003, respectively. In September 2003, he joined the School of Electronic and Electrical Engineering, Hongik University, Seoul, where he is currently a Professor. His research interests include electrically small antennas for wireless communications, reader and tag antenna for RFID, on-glass and conformal antennas for vehicles and aircraft, and array antenna for GPS applications.